Eur. Phys. J. B **7**, 457–466 (1999)

THE EUROPEAN PHYSICAL JOURNAL B
EDP Sciences
© Società Italiana di Fisica
Springer-Verlag 1999

Influence of the interface structure on the barrier height of homogeneous Pb/n−Si(111) Schottky contacts

R.F. Schmitsdorf and W. Mönch[a]

Laboratorium für Festkörperphysik, Gerhard-Mercator-Universität Duisburg, 47048 Duisburg, Germany

Received: 14 May 1998 /Revised and Accepted: 7 September 1998

Abstract. Unreconstructed Pb/n−Si(111) − $(1\times1)^i$ interfaces may be prepared by evaporation of thick Pb films onto Si(111) : Pb−$(\sqrt{3}\times\sqrt{3})$R30° surfaces at room temperature. Current-voltage and capacitance-voltage characteristics of such Pb/n−Si(111)−$(1\times1)^i$ Schottky contacts were measured in the temperature range between 140 and 300 K. The experimental data are analyzed by applying the thermionic-emission theory of inhomogeneous metal-semiconductor contacts as well as the "standard" thermionic-emission theory. From both methods the Schottky barrier height of laterally homogeneous Pb/n−Si(111)−$(1\times1)^i$ contacts results as 0.724 eV. This value is by 74 meV larger than the previously observed barrier heights of laterally homogeneous Pb/n−Si(111)−$(7\times7)^i$ interfaces. Similar differences were reported for $(1\times1)^i$−unreconstructed and $(7\times7)^i$−reconstructed Al- and Ag/n−Si(111) contacts. The reduced barrier heights of all these $(7\times7)^i$ interfaces are explained by the electric dipole associated with the stacking faults of 7 × 7 reconstructions at Si(111) surfaces and interfaces.

PACS. 73.30.+y Surface double layers, Schottky barriers, and work functions – 73.40.Ei Rectification

1 Introduction

Metal contacts are important components of semiconductor devices. Most metal-semiconductor contacts are naturally rectifying [1] and Schottky [2] explained this behavior by a depletion layer on the semiconductor side. The respective barrier height is the energy distance from the Fermi level to the majority-carrier band edge right at the interface and with moderately doped semiconductors the current transport across such Schottky contacts takes place via thermionic emission over the barrier. Quite a number of different physical mechanisms have been suggested to account for the experimentally observed Schottky barrier heights. The extremely controversial discussions go back to the widely held assumption that only one single mechanism controls the barrier heights of metal-semiconductor contacts. Meanwhile, it is commonly accepted that lateral variations of barrier heights exist in almost all real Schottky contacts. This view then corroborates the earlier proposal [3] that one primary and other but then secondary mechanisms explain the experimental Schottky barrier heights.

Ideal metal-semiconductor contacts are considered to be intimate, abrupt, laterally homogeneous, and defect-free, and then the continuum of the metal-induced gap states (MIGS) [4–6] determines their barrier heights. Interface defects and interface dipoles due to foreign atoms or correlated with specific interface structures of substrate atoms may be present in addition to the intrinsic MIG states [7]. Several studies demonstrated the influence of extrinsic interface dipoles that were induced either by interface doping or by specific interface structures.

Aoki and Kawarada [8] and Kampen *et al.* [9] studied hydrogen doping of metal-diamond and Pb/Si(111) contacts, respectively. The interfacial hydrogen lowers the barrier heights of metal contacts on p-type diamond but increases it on p-type silicon. This different behavior was explained by oppositely oriented H–C and H–Si interface dipoles [9,10]. The reason for this is that hydrogen is electropositive with regard to carbon but more electronegative than silicon.

Tung [11] was the first to report on a correlation between atomic interface structures and barrier heights of Schottky contacts. He discovered that the barrier heights of epitaxial $NiSi_2$/n−Si(111) diodes differ by 140 meV depending on the specific interface structures that he called type-A and type-B. High-resolution transmission electron microscopy showed the lattices to be identically aligned on both sides of type-A contacts but to be rotated by 180° around the surface normal for the case of type-B contacts [12]. Later on, Heslinga *et al.* [13] reported a structural dependence of the barrier height of Pb/Si(111) contacts. They evaporated thick lead films onto Si(111)−7 × 7 and Si(111) : Pb−$(\sqrt{3}\times\sqrt{3})$R30°

[a] e-mail: w.moench@uni-duisburg.de

surfaces. From their current-voltage (I/V) characteristics they deduced a barrier-height difference of 230 meV.

The atomic interface structures of buried Pb- and Ag/Si(111) interfaces were investigated using grazing incidence X-ray diffraction (GIXD). After evaporation of more than 100 nm of Ag and Pb onto clean Si(111)–7×7 surfaces at room temperature, Hong *et al.* [14] and Howes *et al.* [15], respectively, found the 7×7 periodicity to be preserved at the interface. The stacking fault in one of the triangular subunits of the 7×7 unit-mesh and by this also the associated corner hole and dimers are still present while the 12 silicon adatoms per unit mesh have vanished. Furthermore, metal overlayers destabilize this $(7\times 7)^i$ interface structure. Hong *et al.* [14] observed that under thick Ag films the $(7\times 7)^i$ interface structure irreversibly converts to a $(1\times 1)^i$ structure during annealing treatments at temperatures above only 250 ℃. The well-known reversible $7\times 7 \leftrightarrow 1\times 1$ transition on clean Si(111) surfaces or, in other words, at vacuum-Si(111) interfaces occurs at 850 ℃. Hong *et al.* [13] and Lucas and Loretto [16] found unreconstructed $(1\times 1)^i$ interfaces when they covered Ag- and $Pb-(\sqrt{3}\times\sqrt{3})$R30°-reconstructed, respectively, Si(111) surfaces with thick films of the same metals at room temperature.

I/V studies showed that the irreversible $(7\times 7)^i \rightarrow (1\times 1)^i$ transition increases the barrier height of Ag/n–Si(111) contacts by approximately 47 meV [17]. This observation was explained by the removal of the stacking fault in the 7×7 unit-mesh. Stacking faults in bulk silicon show a rearrangement of the valence charge [18] that may be described as an electric double layer or, what is equivalent, a dipole layer.

As already mentioned, Heslinga *et al.* [13] investigated the correlation between interface structure and barrier height with Pb/n–Si(111) diodes. Unfortunately, the I/V characteristics of their Pb/n–Si(111)–$(1\times 1)^i$ diodes prepared on Si(111):Pb-$(\sqrt{3}\times\sqrt{3})$R30° surfaces strongly deviated from what is expected for thermionic emission. Therefore, we repeated their experiments and measured I/V and capacitance-voltage (C/V) characteristics of Pb/n–Si(111)–$(1\times 1)^i$ diodes. Our approach differs from the one of Heslinga *et al.* in two essential aspects. First, Heslinga *et al.* obtained clean Si(111) surfaces by thermal decomposition of SiO_2 layers whereas we use H-desorption from Si(111) : H-1×1 surfaces that were prepared by wet chemical etching. And second, our analysis of I/V curves considers lateral inhomogeneities of Schottky barrier heights while Heslinga *et al.* applied standard thermionic-emission theory.

The I/V characteristics of real Schottky diodes generally differ from what is predicted by the theory of thermionic emission. The respective fitting parameter is the so called ideality factor. It may become considerably larger than unity and this indicates that the barrier heights change as a function of the applied voltage. Such behavior will occur when the barrier heights vary laterally and the dimensions of these inhomogeneities are in the order of the depletion-layer width [19–23]. Then, saddle points of the potential occur in front of these patches and their heights will change as a function of applied voltage. The standard analysis of I/V curves thus produces *effective* barrier heights and ideality factors larger than unity. Both parameters vary from diode to diode even if they are identically prepared. Only recently, a linear correlation between effective barrier heights and ideality factors was reported and was attributed to inhomogeneous interfaces [9,17,24]. Barrier heights of homogeneous Schottky contacts were obtained from an extrapolation of the effective barrier heights to the ideality factor characteristic of image-force lowering only. This procedure was justified by numerical simulations [24] that applied theoretical results for inhomogeneous Schottky contacts [22].

In this article we will determine effective barrier heights and ideality factors from experimental I/V curves of Pb/n–Si(111)–$(1\times 1)^i$ contacts by applying the standard theory of thermionic emission. We will compare the extrapolated effective barrier heights with the homogeneous barrier heights directly obtained from the same I/V characteristics by using the theory of thermionic emission over inhomogeneous Schottky barriers. Furthermore, we will explain the barrier-height differences of Pb/Si(111)–$(7\times 7)^i$ and –$(1\times 1)^i$ contacts by the electric dipole of the stacking fault that is a characteristic of Si(111)–7×7 reconstructions on surfaces and at interfaces.

2 On the theory of inhomogeneous Schottky contacts

The "standard" theory of thermionic emission describes the current-voltage relationship of Schottky contacts as [25,26]

$$I_{te}^{stan} = AA_R^{**}T^2\exp\left(-\frac{\Phi_B^{eff}}{k_BT}\right)\left[\exp\left(\frac{e_0V_c}{nk_BT}\right)-1\right], \tag{1}$$

where A is the diode area, A_R^{**} is the effective Richardson constant, T is the temperature, k_B is Boltzmann's constant, e_0 is the electronic charge, V_c is the voltage drop across the space-charge region, and Φ_B^{eff} and n are the effective barrier height at zero bias and the ideality factor of the contact, respectively. In low-doped semiconductors, generation-recombination currents are to be neglected.

In forward direction, the exponential in the square brackets of (1) dominates and it is easily shown that $(1-1/n)$ describes the dependence of the barrier height on the applied voltage. The best-known example of such behavior is the image-force effect that reduces Schottky barriers by [25,26]

$$\delta\Phi_B^{if} = e_0\left(\frac{2e_0^3N_d}{(4\pi)^2(\varepsilon_b\varepsilon_0)^3}(V_{i0}-V_c)\right)^{1/4}, \tag{2}$$

where N_d is the density of dopants, V_{i0} is the interface band-bending with no applied bias, and ε_b and ε_0 are

the static dielectric constant of the semiconductor and the permittivity of vacuum, respectively. For moderate doping, the image-force effect gives ideality factors $n_{if} = 1.01$ to 1.03. Thus, experimental ideality factors n larger than 1.03 cannot be explained by the standard thermionic-emission theory, although large ideality factors are a phenomenon routinely observed with real Schottky contacts. Following an idea of Bastys *et al.* [19] and Tung [21,23] ideality factors larger than n_{if} may be explained by inhomogeneous or "patchy" metal-semiconductor contacts.

Non-uniform Schottky contacts may be modeled by well-separated micro-diodes embedded in an extended region of homogeneous but larger barrier height. The space-charge layer of the surrounding high-barrier-height region will laterally extend into the patches of lower barrier height [27]. If the lateral dimensions of a patch become comparable to or are even smaller than the extension of the depletion layer then the space-charge layers laterally penetrating from opposite edges will overlap. As a result of this, the space-charge potential develops a saddle point in front of the patch and its low barrier height is "pinched-off". The saddle-point barrier height Φ_B^{sad} is intermediate between the values Φ_B^{hom} of the surrounding homogeneous contact area and $\Phi_B^{hom} - \Delta_p$ of the patch right at the interface. The local lowering of the barrier height at the saddle point in front of a circular patch of radius R_p is given by [23]

$$\delta\Phi_p^{sad} = \Phi_B^{hom} - \Phi_B^{sad} = 3\left(\frac{1}{2}\,\frac{\Delta_p}{e_0 V_i}\,\frac{R_p^2}{W^2}\right)^{1/3} e_0 V_i. \quad (3)$$

The term in the nominator represents the dipole moment $\varepsilon_b\varepsilon_0\Delta_p\pi R_p^2$ that is responsible for the lowered barrier height of the patch. The interface band-bending $V_i = V_{i0} - V_c$ depends on the voltage drop V_c across the space-charge layer and the width W of the space-charge layer varies as a function of applied voltage as

$$W = [2\varepsilon_b\varepsilon_0(V_{i0} - V_c)/e_0 N_d]^{1/2}. \quad (4)$$

The variation of the saddle-point barrier as a function of applied voltage is similar to the image-force lowering but differs from the latter effect that is laterally homogeneous. Therefore, sufficiently small patches in Schottky contacts explain ideality factors n larger than $n_{if} = 1.01$ to 1.03. Furthermore, effective barrier heights are expected to be correlated with the ideality factors and to be smaller than homogeneous barrier heights.

Relation (3) suggests to characterize lateral inhomogeneities of Schottky contacts by their individual patch parameters $\gamma_p = 3(\Delta_p R_p^2/4)^{1/3}$. Real Schottky contacts most probably have many patches and their radii R_p and barrier-height deviations Δ_p may vary locally. A reasonable first approximation is a Gaussian distribution of patch parameters γ_p, *i.e.*,

$$N_p(\gamma_p) = \frac{A\rho_p}{\sqrt{2\pi}\sigma_p}\exp\left(-\frac{\gamma_p^2}{2\sigma_p^2}\right). \quad (5)$$

where ρ_p denotes the area density of the patches. The standard deviation σ_p of the distribution may be interpreted as an average patch-parameter

$$\sigma_p = \langle\gamma_p\rangle = 3\langle\left(\Delta_p R_p^2/4\right)^{1/3}\rangle. \quad (6)$$

The integration over the total area of such "patchy" contacts gives the total thermionic-emission current as [23]

$$\begin{aligned} I_{te}^{tot} &= AA_R^{**}T^2\exp\left(-\frac{\Phi_B^{hom}}{k_BT}\right)\left[\exp\left(\frac{e_0(V_a - R_s I_{te}^{tot})}{k_BT}\right) - 1\right] \\ &\quad\times\left\{1 + \frac{4\pi\sigma_p^2\rho_p}{9}\left(\frac{\varepsilon_b\varepsilon_0}{e_0^3 N_d(V_{i0} - V_a + R_s I_{te}^{tot})}\right)^{1/3}\right. \\ &\quad\left.\times\exp\left[\frac{e_0^2\sigma_p^2}{2(k_BT)^2}\left(\frac{N_d(V_{i0} - V_a + R_s I_{te}^{tot})}{\varepsilon_b\varepsilon_0}\right)^{2/3}\right]\right\} \\ &= I_{te}^{hom}(1 + P), \end{aligned} \quad (7)$$

where V_a is the externally applied voltage and R_s is the series resistance. The terms in front of the braces on the right side of (7) are the thermionic-emission current I_{te}^{hom} of a homogeneous Schottky contact of area A, series resistance R_s, and barrier height Φ_B^{hom}. The second term in braces on the right side describes the modification of the I/V curve due to the patches. The patch function P may be rewritten as

$$P = \frac{3\langle\left(\Delta_p\pi R_p^2\right)^{1/3}\rangle^3}{\langle\delta\Phi_p^{sad}\rangle}\rho_p\exp\left[\frac{1}{2}\left(\frac{\langle\delta\Phi_p^{sad}\rangle}{k_BT}\right)^2\right], \quad (8)$$

where the average barrier-height lowering $\langle\delta\Phi_p^{sad}\rangle$ at the saddle-points is defined in analogy to relation (3).

Barrier heights of Schottky contacts may be also determined from capacitance-voltage (C/V) characteristics. The depletion layer capacitance of homogeneous Schottky contacts is obtained as [25,26]

$$C_{dep}^{hom} = \left[e_0^2\varepsilon_b\varepsilon_0 N_d/(e_0V_{i0} - k_BT - e_0V_a)\right]^{1/2}. \quad (9)$$

The extrapolated intercept V_{ext} on the abscissa of an $(1/C_{dep}^{hom})^2$ *versus* V_a plot gives the flat-band barrier height $\Phi_B^{fb} = V_{ext} + (W_{cb} - W_F) + k_BT$. The bulk doping density N_d determines the energy difference $W_{cb} - W_F$ between the conduction-band minimum and the Fermi level in the bulk. Numerical simulations of inhomogeneous contacts [28] showed that their flat-band barrier heights are close to the weighted arithmetic average of their local Schottky barrier heights. The flat-band barrier heights Φ_B^{fb} of Schottky contacts with low patch densities are thus equal to their homogeneous barrier heights Φ_B^{hom} plus image-force lowering $\delta\Phi_B^{if}$ both at zero bias.

3 Experimental

In this investigation, we fabricated Pb/Si(111)$-(1 \times 1)^i$ diodes on low-doped n-type wafers with resistivities between 1 and 10 Ωcm as specified by the supplier

(WACKER Chemitronik). Good ohmic contacts on the rear side of the wafers were achieved by ion implantation of 5×10^{15} As^+-ions per cm^2 with an energy of 150 keV (IMS of the FhG, Duisburg). During the implantation process SiO_2 layers of a thickness of 28 nm grew thermally. Samples measuring 15 mm × 20 mm were cut from these wafers.

We obtained clean Si(111)-7 × 7 surfaces in a two-step process. Wet chemical etching of the samples in a buffered HF solution with pH = 9 (HF : NH_4F : NH_3OH) resulted in hydrophobic and passivated Si(111) : H-1×1 surfaces [29]. Within 6 min after removal from the etch the samples were transferred into a ultrahigh-vacuum system which had an operation pressure of 1×10^{-8} Pa. The hydrogen was desorbed from the surfaces by annealing the samples at 850 °C for 30 s. Only small traces of carbon but no oxygen were detected by Auger electron spectroscopy and low-energy electron diffraction (LEED) showed well-ordered 7×7 patterns. Si(111):Pb-($\sqrt{3}\times\sqrt{3}$)R30° surfaces were prepared by evaporation of 0.4 nm of Pb onto clean 7 × 7 surfaces at room temperature followed by short anneals at 300 °C for 30 s. The surface reconstruction was checked by LEED. Finally, the evaporation of another 150 nm of Pb onto these Si(111):Pb-($\sqrt{3}\times\sqrt{3}$)R30° surfaces resulted in Pb/Si(111)-$(1 \times 1)^i$ diodes. The I/V and C/V measurements were performed outside of the UHV system at room temperature and in the dark. The C/V characteristics were recorded at a frequency of 1 MHz. The exact area of each diode was evaluated by using a microscope.

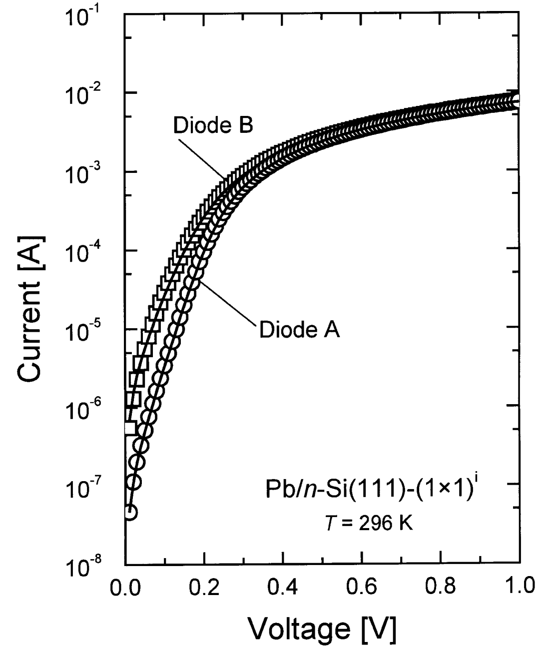

Fig. 1. Forward I/V characteristics of two Pb/$n-$Si(111)$-(1 \times 1)^i$ at room temperature. The full lines are least-squares fits of the thermionic-emission I/V relation (7) for inhomogeneous Schottky contacts to the experimental data. The parameters obtained from this fit and from the application of the "standard" thermionic-emission relation (1) are summarized in Table 1.

4 Results and discussion

4.1 Determination of barrier heights at room temperature

Figure 1 displays the forward current-voltage characteristics of two representative Pb/$n-$Si(111)$-(1 \times 1)^i$ diodes at room temperature. Even though they were identically prepared the contacts exhibit different effective barrier heights and ideality factors. Both quantities were calculated by applying equation (1) to linear regressions of the I/V curves between 0.08 V and 0.13 V. We used the effective Richardson constant $A_R^{**} = 112$ $Acm^{-2}K^{-2}$ of n-type silicon [30] and the diode areas measured 7.85×10^{-3} cm^2. Table 1 shows the Φ_B^{eff} and n values of the two diodes. The contacts are by no means ideal; their ideality factors are larger than n_{if} and their effective barriers differ by more than 10%.

Due to the large scatter of the effective barrier heights obtained from real Schottky diodes it is common practice to take averages. Figure 2 displays histograms of effective barrier heights and ideality factors for as many as 68 Pb/$n-$Si(111)$-(1 \times 1)^i$ diodes. We would like to emphasize that the histograms of Figure 2 are shown here for completeness only because such statistical analysis disregards the pronounced correlation between effective barrier heights and ideality factors [9,17,24]. We will take up this aspect later. For discussions on the fundamental mechanisms of barrier height formation, homogeneous rather than effective barrier heights should be considered only.

The full lines in Figure 1 are least-squares fits of equation (7) to the experimental data. The fitting parameters are the homogeneous barrier height Φ_B^{hom}, the series resistance R_s, the patch density ρ_p, and the standard deviation σ_p of the patch parameter γ_p. The fitting procedure included *all* experimental data in the whole voltage range from 0.01 V up to 1 V. The doping density of each diode was extracted from its individual C/V characteristic that are shown in Figure 3. Table 1 contains the numerical values of the fitting parameters. The homogeneous barrier heights of the two diodes are identical to within 0.7%. However, the diodes differ in that diode B has larger patch density ρ_p and standard deviation σ_p of the patch parameter γ_p than diode A.

The agreement between experimental data and fitted I/V curves in Figure 1 is excellent, *i.e.*, the experimental data are very well described by the thermionic-emission theory of inhomogeneous Schottky contacts. Diodes prepared under identical conditions are expected to exhibit the same homogeneous barrier height Φ_B^{hom}. Therefore, a statistical analysis of homogeneous barrier heights provides an additional test of the model. We performed least-squares fits of equation (7) to the I/V curves of *all* of our 68 Pb/$n-$Si(111)$-(1 \times 1)^i$ diodes. The histogram on the left side of Figure 4 displays the distribution

Table 1. Parameters calculated from the room-temperature I/V and C/V characteristics of the two Pb/n−Si(111)−$(1\times1)^i$ diodes displayed in Figures 1 and 3, respectively.

Diode	Φ_B^{eff} [eV]	n	Φ_B^{hom} [eV]	ρ_p [cm^2]	σ_p [V$^{1/3}$cm$^{2/3}$]	R_s [Ω]	Φ_B^{fb} [eV]	N_d [cm^{-3}]
A	0.701	1.08	0.727	3.3×10^8	1.4×10^{-4}	93.4	0.731	2.51×10^{15}
B	0.625	1.41	0.732	3.7×10^8	1.6×10^{-4}	94	0.718	3.34×10^{15}

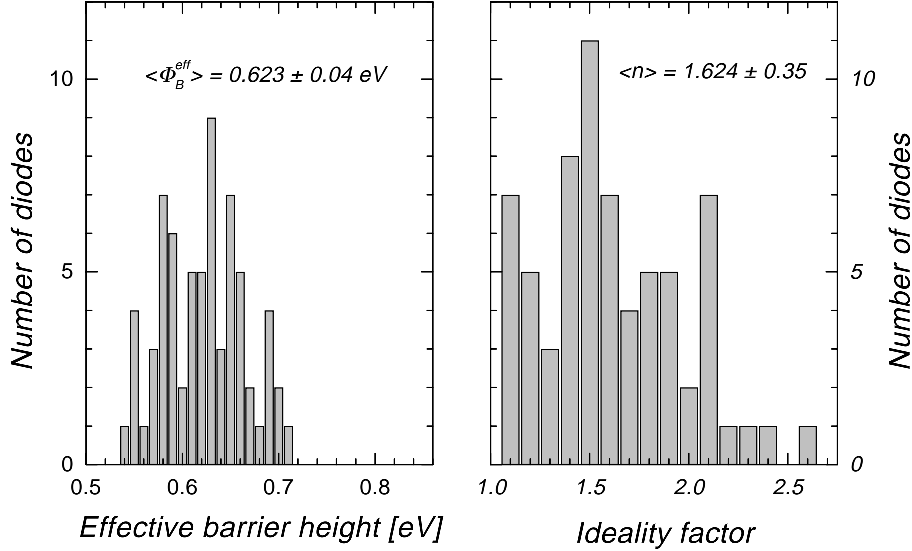

Fig. 2. Effective Schottky barrier heights (left) and ideality factors (right) obtained from forward I/V characteristics of 68 Pb/n−Si(111)−$(1\times1)^i$ diodes obtained from the application of the "standard" thermionic-emission I/V relation (1).

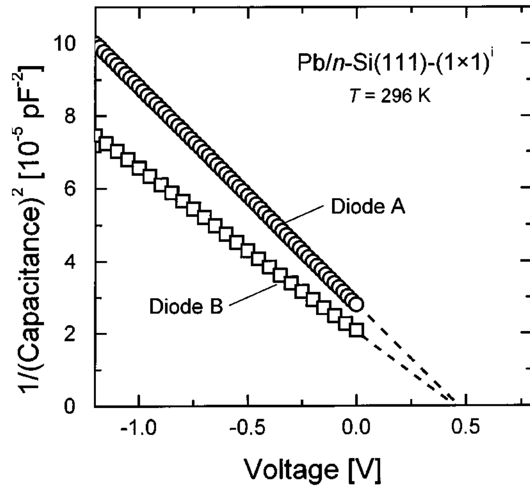

Fig. 3. Capacitance-voltage characteristics of the same two Pb/n−Si(111)−$(1\times1)^i$ diodes of Figure 1. The calculated flat-band barrier heights and doping densities are given in Table 1.

of the homogeneous barrier heights. It is indeed considerably narrower than the distribution of the effective barrier heights of the same diodes shown in Figure 2. The deviations from the average of the homogeneous barrier heights, $\langle\Phi_B^{hom}\rangle = 0.724 \pm 0.02$ eV, might be attributed to the assumptions of the model as, for example, that only circular patch geometries are considered and the patch parameters are assumed to obey a Gaussian distribution. Of course, real diodes can deviate more or less strongly from this idealized picture and the homogeneous barrier heights then seemingly vary.

As mentioned above, the zero-bias barrier heights Φ_B^{hom} obtained from I/V and the flat-band barrier heights Φ_B^{fb} evaluated from C/V characteristics of homogeneous diodes differ by the image-force lowering of the barrier. We also measured the C/V characteristics of our 68 Pb/n−Si(111)−$(1\times1)^i$ diodes and determined the individual donor densities and flat-band barrier heights of each diode. The histogram on the right side of Figure 4 displays all the flat-band barrier heights. Their average is $\langle\Phi_B^{fb}\rangle = 0.744 \pm 0.03$ eV. The average donor density was found as $\langle N_d\rangle = 2.57\times10^{15}$ cm^{-2}. These data and equation (2) give an average image-force lowering of $\langle\delta\Phi_B^{if}\rangle = 18$ meV. This value excellently agrees with the experimental difference $\langle\Phi_B^{fb}\rangle - \langle\Phi_B^{hom}\rangle = 20$ meV. Obviously, the barrier heights obtained from I/V and C/V measurements are consistent if homogeneous instead of effective barrier heights are considered.

Homogeneous barrier heights of Schottky contacts may be determined by fitting equation (7) to experimental I/V curves. Due to the implicit form of equation (7) this procedure requires lengthy calculations. Homogeneous

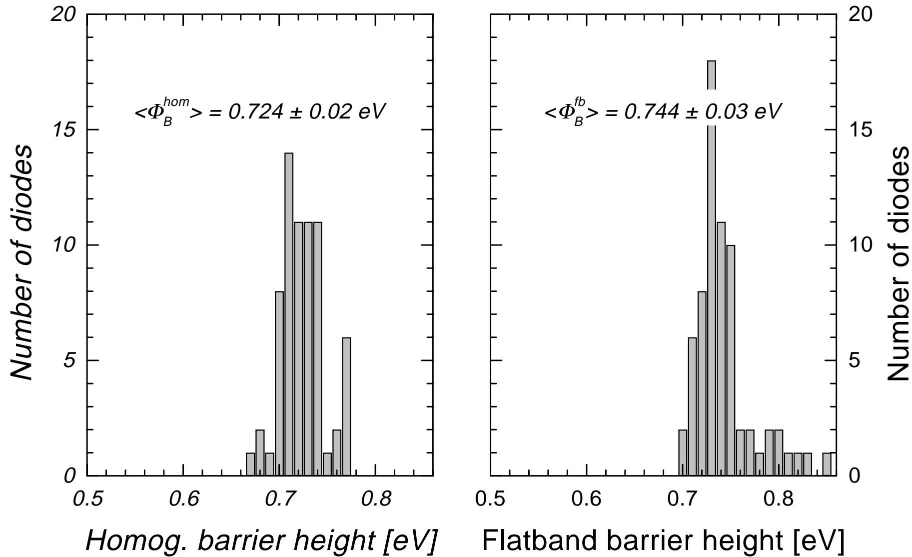

Fig. 4. Homogeneous barrier heights (left) obtained from least-squares fits of thermionic-emission I/V relation (7) for inhomogeneous Schottky contacts to the experimental I/V curves and flat-band barrier heights (right) obtained from capacitance-voltage characteristics of the same 68 Pb/$n-$Si(111)$-(1\times1)^i$ diodes as in Figure 2.

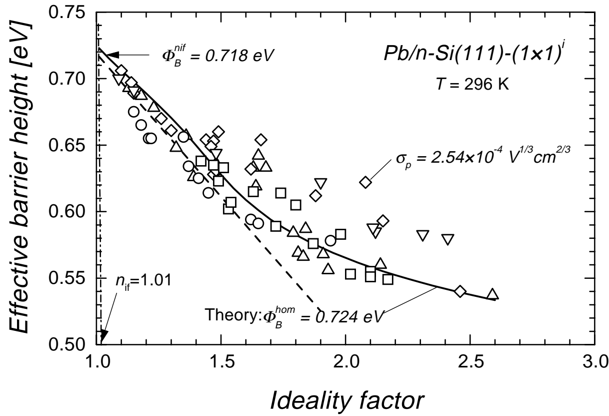

Fig. 5. Effective barrier heights of the same 68 Pb/$n-$Si(111)$-(1\times1)^i$ diodes as in Figure 2 as a function of their ideality factors at room temperature. The full line is a result of numerical simulations (for details see text). Each symbol indicates a different Si(111) substrate.

barrier heights may also be obtained from plots of the effective barrier heights of a set of identically fabricated diodes *versus* their ideality factors [24]. Therefore, Figure 5 shows a plot of the effective barrier heights of all of our 68 Pb/$n-$Si(111)$-(1\times1)^i$ diodes *versus* their ideality factors. The diagram even displays the data of very poor diodes that exhibit very large ideality factors and low effective barrier heights. Figure 5 confirms the well-known correlation [9,17,24,31] between both parameters. The dashed straight line in Figure 5 indicates a linear relationship in the range of low ideality factors $n < 1.4$. An extrapolation to $n_{if} = 1.01$, the "ideal" ideality factor, gives the extrapolated barrier height $\Phi_B^{nif} = 0.718 \pm 0.02$ eV. Within the limits of experimental error the extrapolated barrier height Φ_B^{nif} matches the average of the homogeneous barrier heights $\langle\Phi_B^{hom}\rangle = 0.724 \pm 0.02$ eV obtained from fits of equation (7) to the experimental I/V curves. This agreement gives numerical evidence that homogeneous barrier heights of real Schottky contacts may be extracted from Φ_B^{eff} *versus* n plots that then contain data of many different contacts or from fits of equation (7) to individual I/V characteristics of individual diodes.

To further cross-check our data we simulated I/V curves using equation (7) and the averages $\langle\Phi_B^{hom}\rangle =$ 0.724 eV, $\langle\sigma_p\rangle = 1.92\times10^4$ V$^{1/3}$ cm$^{2/3}$, $\langle N_d\rangle = 2.57\times10^{15}$ cm^{-3}, and $\langle R_s\rangle = 103$ Ω of our 68 Pb/$n-$Si(111)$-(1\times1)^i$ diodes. The patch density ρ_p was stepwise increased from zero to 1.2×10^9 cm^{-2}. To the simulated I/V curves we applied the standard thermionic-emission relation (1) and obtained effective barrier heights and ideality factors. The full line in Figure 5 is the result of this procedure. Obviously, the theoretical curve excellently describes the experimental effective barrier heights over the whole range of ideality factors. Specifically, the $\Phi_B^{eff}(n)$ correlation is linear for ideality factors n smaller than 1.4. In the range of large ideality factors, the curve tends to approach a constant value. Here, the patch density becomes large so that the patches rather than the now small regions in between them almost completely control the current transport. This observation for the first time proofs the theoretical prediction [24] that the effective barrier heights become constant at large ideality factors. The scatter of the experimental data around the simulated line is certainly due to the input parameters of the simulations. As an example, the marked data point in Figure 5 belongs to a diode that exhibits a standard deviation $\sigma_p = 2.54\times10^{-4}$ V$^{1/3}$ cm$^{2/3}$ of the patch parameter. This value deviates by more than 25% from the

mean value $\langle\sigma_p\rangle = 1.92 \times 10^{-4}$ V$^{1/3}$ cm$^{2/3}$ assumed in the simulations.

The average standard deviation $\langle\sigma_p\rangle$ of the patch parameter makes it possible to estimate the mean lowering $\langle\delta\Phi_p^{sad}\rangle$ of the barrier height at the saddle point in front of the patches. For the Gaussian distribution (5) of the patch parameter γ_p assumed, equations (3, 6) show both quantities to be related as

$$\langle\delta\Phi_p^{sad}\rangle = \langle\Phi_B^{hom} - \Phi_B^{sad}\rangle = \sigma_p \left(\frac{2}{e_0 V_i W}\right)^{1/3} e_0 V_i. \quad (10)$$

By considering the above mentioned averages $\langle N_d\rangle = 2.57 \times 10^{15}$ cm^{-3}, $\langle\Phi_B^{hom}\rangle = 0.724$ eV, and $\langle\sigma_p\rangle = 1.92 \times 10^4$ V$^{1/3}$ cm$^{2/3}$ of our 68 Pb/n−Si(111)−$(1 \times 1)^i$ diodes, equation (10) gives $\langle\delta\Phi_p^{sad}\rangle \approx 0.1$ eV. Patches with just this barrier-height lowering at their saddle points would have a diameter of 62 nm what is equivalent to 12% of the depletion layer width W in the homogeneous regions.

In summary, we obtain a Schottky barrier height of 0.72 ± 0.02 eV for homogeneous Pb/n−Si(111)−$(1 \times 1)^i$ contacts that were prepared by evaporation of thick Pb films onto Si(111):Pb-$(\sqrt{3} \times \sqrt{3})$R30° surfaces at room temperature. This means that our experimental results do not support or reproduce barrier heights of 0.93 eV reported by Heslinga *et al.* [13] for such Schottky contacts.

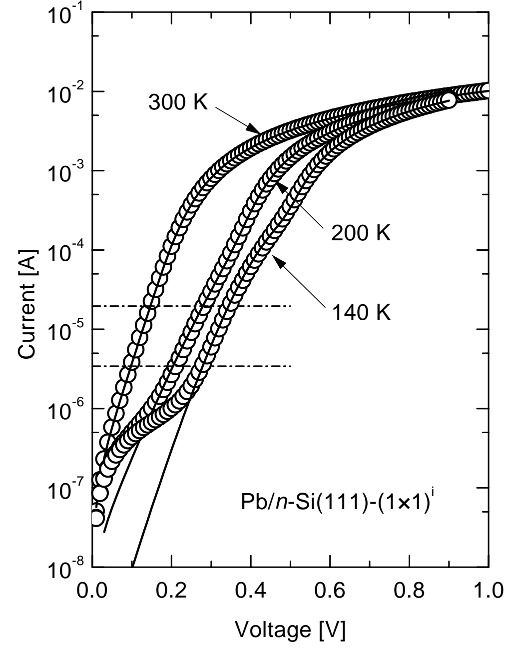

Fig. 6. Forward current-voltage characteristics of a Pb/n−Si(111)−$(1 \times 1)^i$ diode at 140, 200, and 300 K. The full lines are least-squares fits of the thermionic-emission I/V relation (7) for inhomogeneous Schottky contacts to the experimental data.

4.2 Temperature-dependent barrier heights and ideality factors

The effective barrier heights and ideality factors vary not only from one diode to another but also as a function of temperature for individual diodes. When the device temperature is reduced the barrier heights decrease but the ideality factors increase. The "standard" thermionic-emission theory fails to account for this anomaly while the Bastys-Tung thermionic-emission theory of inhomogeneous Schottky contacts [19,23] again explains this familiar behavior.

Figure 6 displays forward I/V characteristics of one single Pb/n−Si(111)−$(1 \times 1)^i$ diode recorded at 140 K, 200 K, and 300 K. The full lines are least-squares fits of equation (7) to the experimental data. The experimental I/V curve measured at 300 K is excellently described by the thermionic-emission model of inhomogeneous Schottky contacts. At lower temperatures shoulders appear in the low-current regimes and the model fails to account for these logarithmic non-linearities. To be more precise, the theoretical relation based on the assumption of circular inhomogeneities and a single Gaussian distribution of patch-parameters does not fit the experimental I/V curves. Recently, Lahnor *et al.* [32] observed similar logarithmic non-linearities with PtSi/Si(111) diodes at low temperatures and argued that the extra current may be fitted by assuming an additional narrow distribution of discrete patch parameters. Our further discussions will neglect these shoulders. At low temperatures and currents larger than 1 μA, on the other hand, the experimental data are rather well described by equation (7) even though the agreement between experiment and theory is not as good as at room temperature. This again indicates that circular patches and a Gaussian distribution of patch parameters is not the optimum approximation. Nevertheless, it is worth mentioning that at 140 K and at an applied voltage of about 0.45 V a distinct shoulder is predicted by the theory that correlates with the inflection of the experimental curve.

Using equation (1), we performed a "standard" analysis of the I/V characteristics recorded as a function of temperature. Figure 7 shows results of two diodes. As usual, the effective barrier heights decrease while the ideality factors increase with decreasing device temperature. The plots of the same data in Figure 8 again reveal a linear correlation of the effective barrier heights and the ideality factors. The extrapolation to the ideality factor n_{if} gives an extrapolated barrier height $\Phi_B^{nif} = 0.70 \pm 0.02$ eV. Within the limits of experimental error this value agrees with the average homogeneous barrier height of the 68 Pb/n−Si(111)−$(1 \times 1)^i$ diodes at room temperature, $\langle\Phi_B^{hom}\rangle = 0.724 \pm 0.02$ eV.

Equations (1, 7) may be also used to simulate the temperature variations of effective barrier heights and ideality factors of inhomogeneous Schottky contacts. For that purpose, we first applied equation (7) to the room-temperature I/V curve displayed in Figure 6 and obtained its homogeneous barrier height Φ_B^{hom}, standard deviation σ_p of the patch parameter γ_p, area density ρ_p of the patches, and series resistance R_s. We inserted these data into equation (7) and calculated I/V curves

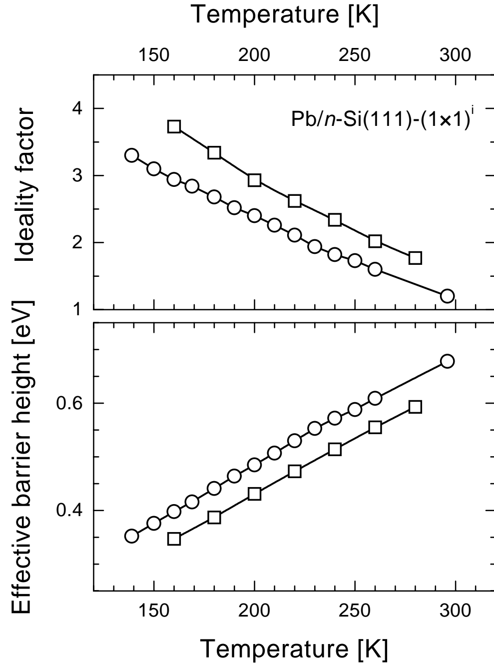

Fig. 7. Temperature variation of effective barrier heights and ideality factors of two Pb/n–Si(111)–$(1\times1)^i$ diodes. The (○) data are for the diode of Figure 6.

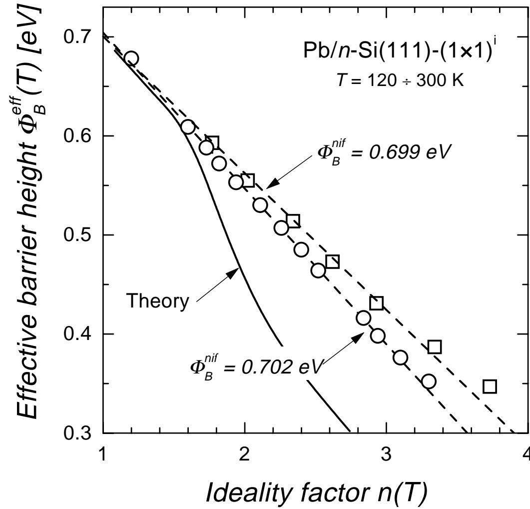

Fig. 8. Effective barrier heights *versus* ideality factors at the same temperature of two Pb/n–Si(111)–$(1\times1)^i$ diodes; same data as in Figure 7. The dashed lines are linear regressions to the experimental data. The full line is a result of numerical simulations (for details see text).

at lower temperatures. Fits of equation (1) to these simulated I/V characteristics again provided effective barrier heights and ideality factors of one inhomogeneous contact but at different temperatures. The full line in Figure 8 is the result of these simulations. For ideality factors n smaller than 1.5 simulated and experimental data agree. The deviations at larger ideality factors are most certainly an artifact of the simplifying assumption made as, for example, that all model parameters are independent of temperature.

Temperature-dependent effective barrier heights and ideality factors were also reported for PtSi/n–Si(111) (Ref. [33]), Au/n–Si(111) (Ref. [34]), Pd_2Si/n–Si(100) (Ref. [35]), Ni/n–GaAs (Ref [36]), and Pt/n–GaAs diodes (Ref. [37]) as well as a commercial Si diode (KYS diode, Ref. [38]). As different as these contacts are their effective barrier heights and ideality factors are always linearly correlated.

4.3 Structure-induced interface dipoles (1×1)

The preceding analysis of experimental I/V curves yielded a homogeneous barrier height $\Phi_{Bn}^{hom}(1\times1) = 0.724$ eV of Pb/n–Si(111)–$(1\times1)^i$ contacts. Kampen and Mönch [9], on the other hand, investigated Pb/n–Si(111)–$(7\times7)^i$ contacts and found a linear correlation between effective barrier heights and ideality factors. An extrapolation to the image-force-controlled ideality factor yielded an extrapolated barrier height $\Phi_{Bn}^{nif}(7\times7) = 0.65$ eV. This value excellently agrees with results reported by Heslinga *et al.* [13] for the same type of contacts. The barrier heights of homogeneous Pb/n–Si(111)–$(7\times7)^i$ and –$(1\times1)^i$ contacts thus differ by $\Phi_{Bn}^{hom}(1\times1) - \Phi_{Bn}^{hom}(7\times7) =$ 74 meV. Similar observations have been reported for Ag- and Al/n–Si(111) contacts by Schmitsdorf *et al.* [17] and Miura *et al.* [39], respectively.

Table 2 summarizes the homogeneous barrier heights of Pb-, Ag- and Al/n–Si(111) contacts with $(1\times1)^i$ and $(7\times7)^i$ interface structures. Obviously, homogeneous n–Si(111)–$(1\times1)^i$ contacts possess barrier heights that are, irrespective of the metal, by 50 to 70 meV larger compared with $(7\times7)^i$-reconstructed interfaces. This observation is attributed to dipoles associated with stacking faults of 7×7 reconstructions. Since this concept was previously discussed in detail [17] only a brief summary will follow.

The clean-surface Si(111)–7×7 reconstruction consists of adatoms and a stacking fault, which is associated with dimers and a corner hole, in one of the two triangular subunits of its unit mesh [40]. As observed by GIXD, the Si adatoms are missing at Ag- and Pb/Si(111)–$(7\times7)^i$ interfaces while the stacking faults are still present. Chou *et al.* [18] calculated the electronic charge distribution of stacking faults in bulk silicon. Figure 9 displays the integrated difference of the calculated charge density over the (111) plane between a crystal with an extrinsic stacking fault and a perfect crystal as well as the atomic positions on the (110) plane. The stacking sequence ...AA′BB′AA′ or, what is equivalent, ...B′BA′AC′C is characteristic of the stacking faults in 7×7-reconstructed Si(111) surfaces and interfaces. The computed distribution of the charge density indicates the existence of an electric double layer associated with the stacking faults of 7×7 reconstructions. At Si(111)–7×7 surfaces and at $(7\times7)^i$-reconstructed metal–Si(111) interfaces as well, the negatively charged silicon atoms of the stacking faults are on the vacuum and the metal side, respectively. This behavior is similar to hydrogen-induced dipoles in Pb/H/Si(111) interfaces

Table 2. Barrier heights of $(1 \times 1)^i$-unreconstructed and $(7 \times 7)^i$-reconstructed, homogeneous metal/n-Si(111) contacts.

Contact	$\Phi_B^{hom}(1 \times 1)$ [eV]	$\Phi_B^{hom}(7 \times 7)$ [eV]	$\delta\Phi_B^{hom}(7 \times 7)^i$ [meV]
Pb/n−Si(111)	0.724[a]	0.65[b]	−74
Ag/n−Si(111)	0.742[c]	0.695[c]	−47
Al/n−Si(111)	0.75[d]	0.68[d]	−70

[a] This work. [b] From references [9,13]. [c] From reference [17]. [d] From reference [39].

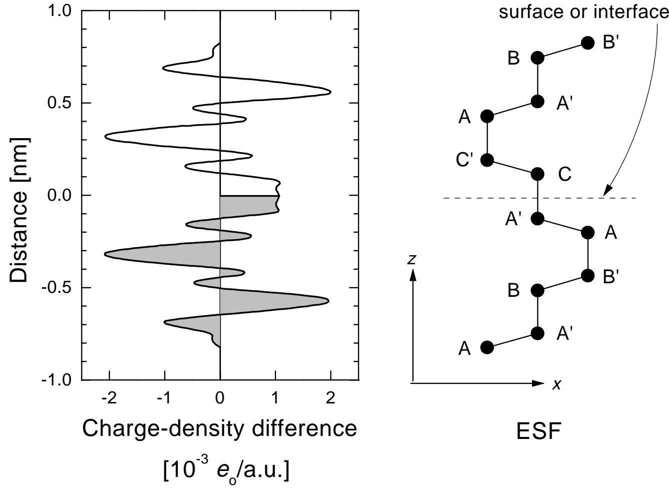

Fig. 9. Integrated difference of the charge density over (111) planes between a silicon crystal with an extrinsic stacking fault (ESF) and a perfect silicon crystal and atomic positions in the (110) plane. (1 a.u. $= a_{Bohr}^3 = 1.48 \times 10^{-4}$ nm^3). After reference [18].

since hydrogen is more electronegative than silicon. Interfacial hydrogen lowers the barrier heights of Pb/n−Si(111) contacts [9] and, therefore, it is plausible that the stacking faults of $(7\times7)^i$-reconstructed metal–Si(111) interfaces also reduce the barrier heights in comparison to unreconstructed $(1 \times 1)^i$ interfaces. The lowering of the barrier height induced by stacking faults may be easily estimated.

The potential drop across a dipole layer may be written as

$$\delta U_{dip} = \pm p_a/\varepsilon_i\varepsilon_0, \tag{11}$$

where p_a is the dipole moment per unit area. In the case considered here, ε_i is an interface dielectric constant that considers the screening by the MIGS. A numerical integration of the theoretical charge-density difference associated with stacking faults in silicon as displayed in Figure 9 gives a dipole moment per unit area of

$$p_a^{7\times7} = 4.93 \times 10^7\ [e_0\,\mathrm{m/m^2}] = 7.89 \times 10^{-12}\ [\mathrm{C/m}].$$

Relation (10) then yields a $(7 \times 7)^i$-induced lowering of the barrier height at metal/n–Si(111) contacts of

$$\begin{aligned}\delta\Phi_{Bn}^{hom}(7 \times 7)^i &= \Phi_{Bn}^{hom}(7 \times 7)^i - \Phi_{Bn}^{hom}(1 \times 1)^i \\ &= -e_0 p_a^{7\times7}/2\varepsilon_i\varepsilon_0 = -0.445/\varepsilon_i\ [\mathrm{eV}].\end{aligned}$$

The factor 1/2 accounts for the fact that only one half of the $(7\times7)^i$ unit mesh contains the stacking fault. A range of $\delta\Phi_{Bn}^{hom}(7 \times 7)^i$ may be estimated by choosing the bulk dielectric constant $\varepsilon_i = \varepsilon_b = 11.9$ as upper and $\varepsilon_i \approx 4$ as lower limits of the interface dielectric constant. Ludeke *et al.* [41] estimated the latter value for metal-GaAs contacts. These choices then give a range of 37 meV $\leq \delta\Phi_{Bn}^{hom}(7 \times 7)^i \leq$ 110 meV for the barrier-height lowering induced by the $(7 \times 7)^i$ stacking faults. Obviously, this estimate is in remarkably good agreement with the experimental data and thus strongly supports the present interpretation that the lower barrier heights of $(7 \times 7)^i$-reconstructed metal–Si(111) interfaces in comparison to unreconstructed $(1 \times 1)^i$ contacts are due to interface dipoles associated with the stacking fault of the $(7 \times 7)^i$ interface structures.

5 Conclusions

Thermionic emission over the barrier governs the current transport across rectifying metal-semiconductor contacts on moderately doped semiconductors. It is well known since long that the simple thermionic-emission theory provides no adequate description of the forward I/V characteristics of even carefully prepared real Schottky contacts. Therefore, the standard analysis of forward I/V curves uses *effective* barrier heights that depend on the applied voltage. An additional phenomenologically introduced parameter, the so called *ideality factor*, characterizes this behavior. Patches of reduced barrier height and dimensions in the order the depletion-layer widths provide a reasonable physical explanation of this voltage dependence of barrier heights. A most simple approach assumes circular patches and a Gaussian distribution of their patch parameters γ_p. The present study which included 68 seemingly identically prepared Pb/n−Si(111)−$(1\times1)^i$ contacts confirmed this simple thermionic-emission theory of laterally inhomogeneous Schottky contacts. The Pb/n−Si(111)−$(1\times1)^i$ contacts were found to have a homogeneous barrier height of 0.72 ± 0.02 eV. This value was obtained both by directly applying the theoretical current-voltage relationship derived by Tung for thermionic emission at inhomogeneous contacts and by extrapolation of effective barrier heights to the ideality factor that is determined by the image-force lowering only. Extensive simulations confirmed the pronounced correlation between effective barrier heights and ideality factors. These procedures provide reliable Schottky barrier heights of

homogeneous metal-semiconductor contacts by fits of thermionic-emission theory to forward I/V curves of real and then inhomogeneous contacts.

However, it should to be kept in mind that even homogeneous Schottky contacts are not necessarily ideal. As an example, the homogeneous barrier heights of $(1 \times 1)^i$-unreconstructed and $(7 \times 7)^i$-reconstructed Al-, Ag-, and Pb/n–Si(111) interfaces differ by approximately 65 meV irrespective of the metal. The lower barrier heights of the $(7 \times 7)^i$ contacts are explained by the dipole associated with the stacking fault of the $(7 \times 7)^i$ interface reconstruction. Theoretical Schottky barrier heights of *ideal* metal-semiconductor contacts should be only compared with experimental data of homogeneous $(1 \times 1)^i$-unreconstructed interfaces.

The authors are grateful to Dr. Graeff of WACKER Chemitronik in Burghausen for supplying the silicon wafers. This work was partly supported by grants Mo318/16–1&2 of the Deutsche Forschungsgemeinschaft.

References

1. F. Braun, Pogg. Ann. Physik **153**, 556 (1874).
2. W. Schottky, Naturwissenschaften **26**, 843 (1938).
3. W. Mönch, Phys. Rev. Lett. **58**, 1260 (1987).
4. V. Heine, Phys. Rev. A **138**, 1689 (1965).
5. S.G. Louie, M.L. Cohen, Phys. Rev. B **13**, 2461 (1976).
6. E. Louis, F. Yndurain, F. Flores, Phys. Rev. B **13**, 4408 (1976).
7. For more details the reader is referred to the monograph by W. Mönch, *Semiconductor Surfaces and Interfaces*, 2nd ed. (Springer, Berlin 1995).
8. M. Aoki, H. Kawarada, Jpn J. Appl. Phys. **33**, 708 (1994).
9. T.U. Kampen, W. Mönch, Surf. Sci. **331-333**, 490 (1995).
10. W. Mönch, Europhys. Lett. **27**, 479 (1994).
11. R.T. Tung, Phys. Rev. Lett. **51**, 461 (1984).
12. D. Cherns, G.R. Anstis, J.L. Hutchinson, J.C.H. Spence, Philos. Mag. A **46**, 849 (1982).
13. D.R. Heslinga, H.H. Weitering, D.P. van der Werf, T.M. Klapwijk, T. Hibma, Phys. Rev. Lett. **64**, 1589 (1990).
14. H. Hong, R.D. Aburano, D.S. Lin, H. Chen, T.-C. Chiang, Phys. Rev. Lett. **68**, 507 (1992).
15. P.B. Howes, K.A. Edwards, D.J. Hughes, J.E. Macdonald, T. Hibma, T. Bootsma, M.A. James, Phys. Rev. B **51**, 17740 (1995).
16. C.A. Lucas, D. Loretto, Surf. Sci. **344**, L1219 (1995).
17. R.F. Schmitsdorf, T.U. Kampen, W. Mönch, Surf. Sci. **324**, 249 (1995).
18. M.Y. Chou, M.L. Cohen, St.G. Louie, Phys. Rev. B **32**, 7979 (1985).
19. A.I. Bastys, V.B. Bikbaev, J.J. Vaitkus, S.C. Karpinskas, Litovskii Fizicheskii Sbornik **28**, 191 (1988).
20. J.H. Werner, H.H. Güttler, J. Appl. Phys. **69**, 1522 (1991).
21. R.T. Tung, Appl. Phys. Lett. **58**, 2821 (1991).
22. J.P. Sullivan, R.T. Tung, M.R. Pinto, W.R. Graham, J. Appl. Phys. **70**, 7403 (1991).
23. R.T. Tung, Phys. Rev. B **45**, 13509 (1992).
24. R.F. Schmitsdorf, W. Mönch, J. Vac. Sci. Technol. B **15**, 1221 (1997).
25. S.M. Sze, *Physics of Semiconductor Devices*, 2nd ed. (Wiley, New York, NY, 1981).
26. E.H. Rhoderick, R.H. Williams, *Metal-Semiconductor Contacts*, 2nd ed. (Clarendon, Oxford, 1988).
27. E. Wasserstrom, J. McKenna, Bell Syst. Techn. J. **49**, 853 (1970).
28. J.P. Sullivan, R.T. Tung, M.R. Pinto, J. Appl. Phys. **70**, 1703 (1991).
29. P. Dumas, Y.J. Chabal, G.S. Higashi, Phys. Rev. Lett. **65**, 1124 (1990).
30. M.P. Lepselter, S.M. Sze, Bell. Syst. Techn. J. **47**, 195 (1968).
31. P. Werner, W. Jäger, A. Schüppen, J. Appl. Phys. **74**, 3846 (1993).
32. P. Lahnor, K. Seiter, M. Schulz, W. Dorsch, R. Scholz, Appl. Phys. A **61**, 369 (1995).
33. J.H. Werner, H.H Güttler, J. Appl. Phys. **69**, 1522 (1991).
34. T.P. Chen, T.C. Lee, C.C. Ling, C.D. Beling, S. Fung, Solid-St. Electron. **36**, 949 (1993).
35. S. Chand, J. Kumar, Appl. Phys. A **63**, 171 (1996).
36. M. Nathan, Z. Shoshani, G. Ashkinazi, B. Meyler, O. Tolotarevski, Solid-St. Electron. **39**, 1457 (1996).
37. H.-W. Hübers, H.P. Röser, J. Appl. Phys. **84**, 5326 (1998).
38. S.S. Simeonov, E. Kafedjiiska, Semicond. Sci. Technol. **12**, 1016 (1997).
39. Y. Miura, S. Fujieda, K. Hirose, Phys. Rev. B **50**, 4893 (1994).
40. K. Takayanagi, Y. Tanishiro, M. Takahashi, S. Takahashi, Surf. Sci. **164**, 367 (1985).
41. R. Ludeke, G. Jezequel, A. Taleb-Ibrahimi, Phys. Rev. Lett. **61**, 601 (1988).